



Aquifer Delineation and Groundwater Potential Assessment in Ayegbaju Ekiti

Onwuka, O.J* and Daramola, C

Department of Geophysics, Federal University Oye-Ekiti

Corresponding Author: Julius.onwuka@fuoye.edu.ng

Abstract

This study investigates aquifer types and distribution in Ayegbaju Ekiti using 2D imaging and vertical electrical sounding (VES) techniques to mitigate overdependence on a single groundwater source. Hydro-geophysical parameters, including aquifer resistivity, thickness, and depth, were identified through 1D models and 2D pseudosections. Resistivity values for the first layer ranged from 162.5 to 191.8 ohm-m with a thickness of 1.1 – 2.0 meters. The second layer showed resistivity of 123.0 – 3988.8 ohm-m and thickness of 1.2–5.2 meters, while the third layer had resistivity of 96.5–9094.5 ohm-m and thickness of 5.3 – 6.9 meters. Basement layers, at depths of 7.5 – 12.5 meters, exhibited high resistivity (>150 ohm-m). The pseudo-section revealed fracture zones, crucial for groundwater accumulation, with resistivity varying from 89 to 874 ohm-m. Despite the area's low water zone classification, VES 2 is promising for groundwater exploration, offering appreciable aquifer thickness and depth.

Keywords: Pseudosections, Aquifer, Hydro-geophysical characterisation, Fracture Zone

Introduction

Subsurface evaluation is crucial in the quest for water, particularly in Ayegbaju, which has a complicated geological foundation. In groundwater exploration, an aquifer is defined as a geological formation of rock and/or silt that contains groundwater. Groundwater refers to rainwater that has permeated the soil beyond the surface and accumulated in subterranean voids. The numerous successes of groundwater investigations utilising electrical resistivity techniques (ERT), specifically the vertical electrical sounding (VES) method, were aimed at examining the anomalous subsurface conditions and the rock competency and structures present in the study area. Recent studies have used various geophysical and remote sensing techniques to evaluate groundwater potential in different regions of Africa, including Ekiti State, Nigeria. Fajana et al. (2024) used aeromagnetic and remote sensing data to map geological structures linked to groundwater assessment in five locations, including Ayegbaju, Ekiti. Their findings highlighted topography, drainage patterns, and magnetic anomalies indicating subsurface formations favorable for groundwater accumulation. Walraevens et al. (2025) investigated groundwater potential in five African regions covering Ethiopia, Tanzania and Libya utilizing combined techniques. Their findings on inter-basin deep groundwater flow challenged traditional water balance assumptions. Zenande et al. (2024) used GIS, remote sensing and Analytical Hierarchical Process (AHP), to evaluate the groundwater potential in the

Ntabankulu municipality, Eastern Cape, South Africa. Findings from the study classified the groundwater potential zones as: very poor (11.06%), poor (25.36%), moderate (26.73%), good (22.72%), and very excellent (11.93%). A reasonable accuracy forecast of 61% was obtained via validation using 242 existing boreholes and area under the curve (AUC) analysis. In De Aar, Northern Cape, South Africa, Baloyi et al. (2024) used hydrogeophysical techniques, including Vertical Electrical Resistivity Sounding (VES) and ground telluric methods, to identify unconfined and confined aquifers. Their study revealed a double-layer aquifer system with resistivity values ranging from 0.9–177 Ω m and groundwater levels above 50 m, highlighting the need for improved recharge assessments. In Kaduna, Nigeria, Alao et al. (2023) used the electric resistivity technique with 60 vertical electrical sounding points to evaluate groundwater potential. According to their research, aquifers that are 30 to 59 meters deep and have hydraulic conductivity levels between 0.337 and 10.62 meters per day are safer to draw water from. In contrast, shallow aquifers (8–14 m) were more vulnerable to contamination and less suitable for sustainable groundwater development. As demonstrated by Oyedele et al. (2009), researchers have extensively used Electrical Resistivity Tomography (ERT) for the analysis of groundwater, earth sciences, engineering, and environmental challenges. The data collected from three vertical electrical sounding (VES) stations was analysed, and

the results were shown as tables, figures, and curves. To guarantee the success of the project, the geophysical data gathered during the survey serves as the basis for defining the region's geology and other lithological characteristics.

1.1 Geology of the area and its environs

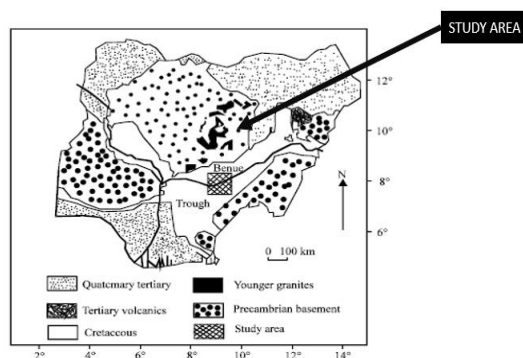


Figure 1: Study area as indicated on Geological map of Nigeria from Precambrian basement to Cretaceous sediments (Modified after Onyedim, 2007).

Figure 1 showed the geologic map of Nigeria showing the Precambrian basement to Cretaceous sediments while figure 2 showed the coloured characterisation of the major Nigerian geological terrain including the sedimentary Basin incorporated with the basement complex having the Niger Basin on the down left (pink) and Chad Basin on top right (yellow).

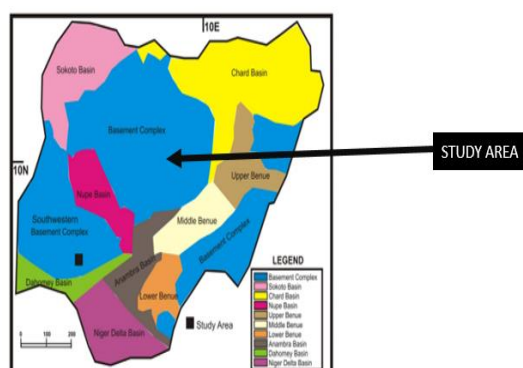


Figure 2: Major geological Terrains of Nigeria including the sedimentary Basin and Basement complex (Modified after Rahaman, 1988) showing the study area.

Nigeria's geology comprises the Basement Complex, which is pan-African and exceeds 600 million years in age (Precambrian), the Younger Granites, which date to the Jurassic period (200–145 million years old), and the Sedimentary Basins, which range from Cretaceous to Recent epochs. According to Rahman (1976), the Archean and Proterozoic eons of the Precambrian are when Nigeria's geology first began to form. The Precambrian igneous and

metamorphic crystalline basement rock that makes up the Nigerian Province. Nigeria's earliest Precambrian rocks dating to the Archean or Paleoproterozoic, and consists mostly of Beninian gneiss. The Nigerian Province refers to the crystalline foundation rock of the nation, which is an extension of the central Hoggar reactivated basement. Schist, migmatite, garnet, sillimanite, kyanite, and staurolite are present in this complex, together indicating high-grade metamorphism that reached the amphibolite stage within the metamorphic facies sequence. The metamorphism of granulite facies and charnockite formations is associated with granites. In the southwest, near Ibadan, the Migmatite-Gneiss Complex has distinct characteristics. The metamorphosis of greywacke, shale, and interbedded sandstones resulted in the formation of banded gneiss, schist, and quartzite. Metamorphosed traces of a tholeiitic magma series are retained in some amphibolite strata. During the Liberian orogeny, some 2.75 billion years ago, the Ibadan area saw initial bending and metamorphism. The Eburnean orogeny, occurring 2.2 billion years ago, was followed by more intense deformation. The Proterozoic metazquartzites in the Ibadan area are overlain by pelite schist, interspersed with magnesium-rich mafic sills. The Older Granites in Nigeria include intrusions of granite, syenite, and diorite, originating from the Pan-African Orogeny and produced between 700 and 500 million years ago. The Paleozoic era (541-251 million years ago) saw the formation of volcanic debris-filled molasse grabens during the Cambrian period, coinciding with the beginning of the Paleozoic, when the Older Granites were deposited, resulting in the formation of dacite and Shoshone. Granite intrusions have sometimes generated substantial batholiths and charnockite. Dikes composed of dolerite and basalt were introduced concurrent with the conclusion of the Pan-African orogeny. Southern Nigeria has extensive sedimentary basins partitioned by the Okitipupa Ridge. It was not until the Albian epoch of the Cretaceous that the basins began to accumulate material. The 600-meter-thick Odukpai Formation in present-day Calabar was formed during the Cenomanian to early Turonian period. It consists of arkose sandstone, limestone, and shale. The blue-gray shales and marl limestone of the Awgu Formation are dated to the Coniacian, but the Eze-Aku Formation is assigned to the Turonian based on fish teeth, ammonites, and echinoids. Sea levels fell during the Cretaceous Santonian age. Shale, mudstone, limestone, and sandstones formed in an offshore environment are however recorded in the Nkporo Formation by the Campanian and Maastrichtian eras.

In different regions of Nigeria, the Owelli Sandstone, Enugu Shale, and Asata Shale all formed at roughly the same time in shallow water environments. The Mamu Formation coals from the Maastrichtian and the Nsukka Formation, both of which contain ammonites, are other formations of a comparable age. The Abeokuta Formation was formed in southwest Nigeria during the Maastrichtian period because to a notable sea incursion. Nigeria encompasses around ten percent of the Chad Basin. Albion Bima sandstone overlays Precambrian foundation rock, followed by Turonian limestone and shale layers of the Gongila Formation. The Senonian is the period during which the marine shales of the Fika Formation were created. The Gombe Sandstones, interspersed with ironstone, siltstone, and shales, were deposited due to changes in the estuarine environment induced by the Maastrichtian period. The Cenozoic era spans from 66 million years ago to the present, characterised by elevated sea levels even in its early phase. During the Paleocene, the Akinbo Formation and Ewekoro Formation were deposited in the west, and the Ino Formation, characterised by thick layers of clay shale, developed above the Nsukka in the east. Marine sediments are present in the Sokoto Group in the Iullemeden Basin. As sea levels started their decline throughout the Eocene, Nigeria mostly underwent terrestrial sedimentation. In the Chad Basin, sedimentary strata underwent folding into anticlines and synclines from the conclusion of the Cretaceous until the beginning of the Cenozoic. Erosion resulted in an unconformity in younger strata. The Chad Formation consists of Pliocene lake deposits, succeeding the Paleocene Kerri Kerri Formation, which was created from terrestrial sediments, according to Schluter (2006).

Review of Water exploration and Electrical Method

Given the significant role water plays in all aspects of life, accurate groundwater assessment and subsurface evaluation are essential to human existence. This work was motivated by the requirement for high-quality water availability, particularly in a terrain with many basements like our study area. The diverse outcomes and conclusions of groundwater investigations, encompassing the vertical electrical sounding (VES) technique, electrical resistivity technique (ERT), geophysical methods, and structures functioning as aquifer reservoirs, were utilised to examine the anomalous subsurface conditions in the study area. Onwuka et al. (2022) indicated that researchers used ERT for analyses in earth science, engineering, and environmental subjects. The geophysical data

collected during in-situ observation is crucial for characterising the location, assuring safety, and offering remedies to the anomalous effect under examination. Groundwater investigation and aquifer protective capacity delineation have both benefited from the use of geophysics over the years. Abu El-Magd and Eldosouky (2021), integrated with process, various techniques, models, imaging, and other integrated approach for evaluating groundwater potentiality. An "aquifer" is a piece of porous, permeable rock that can easily store water and transport it to wells and streams. According to both Ehirim and Ebeniro (2010) and Ugwuanyi et al. (2015), the primary source of potable water for household, commercial, and agricultural purposes as of 2015 is identified as such. Hasan et al. (2021) assessed subsurface lithology, groundwater vulnerability, and aquifer protective capacity by 68 vertical electrical sounding investigations. Data was analysed with the 1D inversion program 1X1D to generate spatial distribution maps with ArcGIS 10.5. The analysed region had three to four subsurface geoelectric layers, and the geographical distribution maps for AR indicated that the quality of fresh groundwater contributed to an increased production potential. Utilising aquifer resistivity and thickness data, hydrogeological maps depicting hydraulic conductivity and transmissivity variations were generated by Obiora et al. (2016) to assess the aquifer characteristics and distribution in the northern region of Paiko, Nigeria, which possesses a prolific aquifer. Obiora et al. (2018) also assessed the changes and interrelations of several parameters of a sandstone formation using the Schlumberger electrode configuration in Ninth Mile area of southeastern Nigeria. Eugene-Okorie et al. (2020) conducted a Vertical Electrical Sounding (VES) in Oraifite, Southeastern Nigeria, to evaluate groundwater potential and aquifer susceptibility. The data were analysed using WINRESIST software, yielding geoelectric curves that indicate the resistivities, depths, and thicknesses of each geoelectrical layer. Dar Zarrouk parameters and aquifer transmissivity were computed using the values of aquifer resistivity and thickness. From the results, variations of the computed parameters were observed. The average value of the aquifer's resistivity, which ranges from 420.1 to 27,585.8 m, is 4906.3 m, while the range of its thickness is 13.4 to 93.9 m. The transverse resistance varies from 29,388.88 to 1,158,604.0 m², the longitudinal conductance spans from 0.0015 to 0.2136 S, and the transmissivity extends from 1.1692 to 123.7905 m²/day. The findings of this research served as a reference for extensive groundwater management. A related study by Amadi et al. (2011)

in Gidan Kwano, Niger State showed that the area has five geo-electric layers, with the uppermost soil layer exhibiting high resistivity and a thickness between 0.3 and 1.6 meters. The worn basement aquifer and the cracked basement aquifer were identified, indicating that these aquifer units may possess considerable groundwater potential, with a thickness of about 4.3 meters.

1.2 Study Area

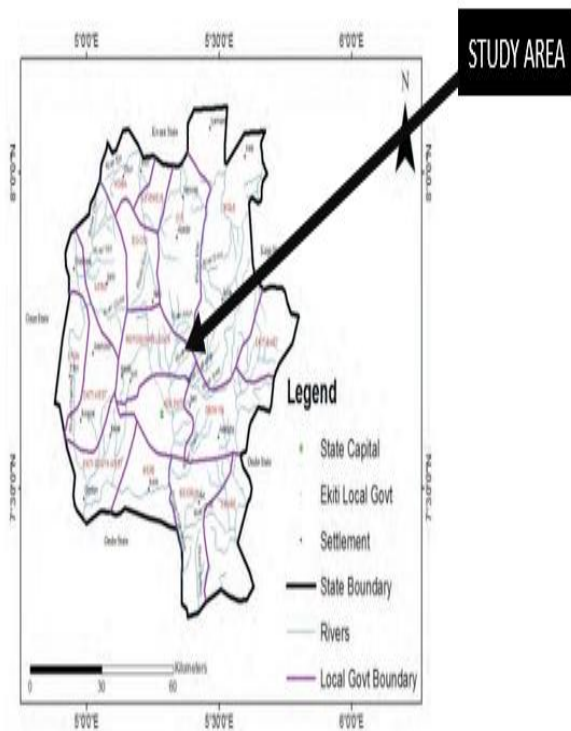


Figure 3: Map of Ekiti showing the study area (Modified after Bayowa et al., 2014) showing the study area.

Figure 3 illustrates the geographical position of the research region, located along Ayegbaju-Ekiti, while Figure 4 presents the base map used for the study, complete with coordinates. The study area is delineated by Ilejemeje LGA to the north, Irepodun/Ifelodun LGA to the south, Ikole LGA to the east, and Ido/Osi LGA to the west, as illustrated in Figure 3. Rahaman et al. (1988) recorded the coordinates of the entire region, with latitude ranging from 7.52220E to 7.52222E and longitude from 8.62129N to 8.62098N UTM. It is accessible through various footpaths and major and minor roads. The topography is gently undulating, identified series of valleys and falls within the tropical rain forest with distinct wet (between November and April) and dry (May and October) seasons, whereas the mean monthly temperature is about 28°C while the mean

humidity is over 70%, and the mean annual rainfall is about 1800 mm. Rock types found in the study area include migmatite, porphyritic granite/coarse porphyritic biotite, and biotite hornblende granite. The rock types are made of Precambrian to Cambrian crystalline basement complex involving, Pan-African older granitoid, metasedimentary/meta-igneous rocks, and migmatite-gneiss complex, Rahaman (1976).

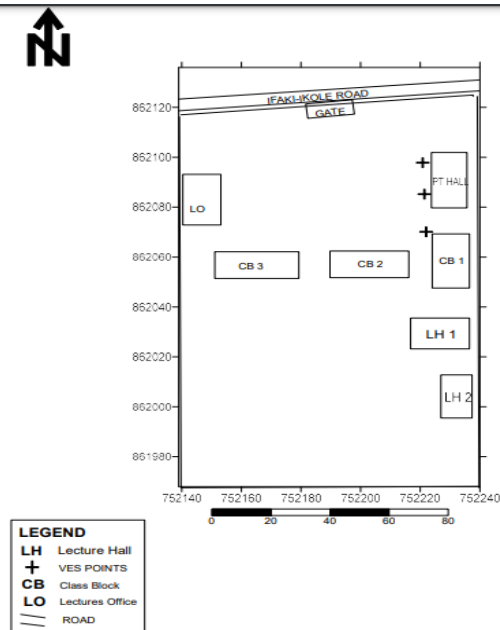


Figure 4: Base Map for Study Area (Modified after Daramola, 2023).

2.0 MATERIALS AND METHOD

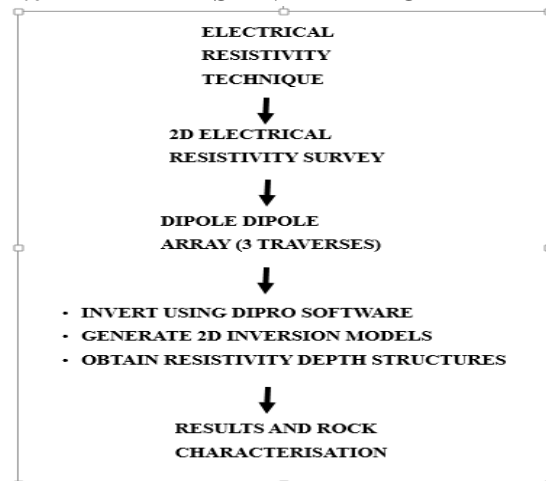


Figure 5: Research Workflow



Figure 6: Resistivity meter and other field equipment used.

Figure 4 is the research's base map, which displays the VES locations and the water exploration region. Figure 5 shows the study procedure that was used. The tools used for the electrical technique geophysical survey are shown in Figure 6 and these include; the resistivity meter (ABEM Terrameter SAS 1000), connecting cables, the recording sheet, hammer, reel lines and electrodes. The electrodes are tiny steel metal rods that are around half a metre long. They have one sharp end that allows them to be pushed firmly into the ground for excellent electrical contact. The reel lines were used to determine the optimal spacing for array arrangement. These lines were pre-labeled with the correct arrangement for the current and potential electrode placement. It was used to evaluate each traverse's straightness. The measurement began with a "1a" gap between the C1-C2 (and likewise the P1-P2) electrodes in the electrode setup. The first series of measurements maintains the C1-C2 dipole pair spacing at "1a" while setting the "n" factor, which calculates the ratio of the distance between the C1-P1 electrodes to the C1-C2 dipole spacing, to 1. The C1 electrode is twice as far away from the P1 electrode as the C1-C2 dipole pair is separated when "n" equals 2. Accurate potential measurements become difficult when the "n" spacing factor is increased to a maximum of 6 because of the very low potential values. A second series of measurements was made with different values of "n," extending the distance between the C1 and C2 dipole pair to "2a" in order to further explore the matter. The device measured the middle point between the current and potential dipoles. The placements of the current and potential electrodes are aligned using constant electrode "a" spacing. To change the depth range of the measurement, the current and potential electrodes were both shifted outward. Three traverses, each measuring 65 meters in length, were created to save space because of the adjacent lecture building. Traverses 1 and 2 were positioned parallel to the

region being studied, whereas Traverse 3 was positioned perpendicular to the research site. The base map in figure 4 shows the location of the traverses, which were between the geographic grid of 7.82224° E, 7.82216° E Easting and Northings 8.61974° N, 8.62019° N.

Data Acquisition

During the survey, values were automatically generated by the ABEM Terrameter SAS (Self Averaging System) 1000, which performed automatic recordings of both voltage and current, compiled the results, computed resistance in real time, and displayed it digitally. As noted by Dobrin and King (1976) and Alile et al. (2011), the system was configured to simultaneously display apparent resistivity and induced polarisation data. The direct-current electrical survey was employed in the data acquisition after Keller and Frischknecht (1966), Telford et al. (1990), and Hallof (1957). Ohm's law was used to compute the apparent resistivity ρ_a in ohm-meters ($\Omega\cdot m$): $\rho_a = 2\pi n \Delta v$, where n is the distance between the electrodes in meters and Δv is the measured potential difference in millivolts (mV). The apparent resistivity data was obtained by graphing the recorded values at the array midpoints at depths that corresponded to a certain fraction, usually 1/3 or 1/2 of the array spacing.

Data Processing and Interpretation

An automated two-dimensional resistivity model of the subsurface electrical geology was created using the data gathered. The qualitative assessment of the traversal is based on these statistics. Both parallel and perpendicular orientations were used to create the traverse. The contouring of the resistivity values illustrates changes in apparent resistivity along the survey line. This map is termed a pseudosection due to the inaccuracy of the depths shown. Dahlin (1993). Pseudosections serve as valuable instruments for qualitative analysis and quality control, despite the inability to directly derive accurate depth information from them. Dahlin and Loke (1998). Each traversal had three VES stations, with electrode spacing (AB/2) varying from 1 to 65 meters. Depth sounding curves were generated by plotting the apparent resistivity values versus electrode spacing (AB/2) on a bi-logarithmic graph sheet. The curve type was subsequently ascertained via visual inspection of the field curves. Partial curve matching was conducted on the field curves. For one-dimensional computer-assisted interpretation, the interpretation results (layer resistivity and thicknesses) were entered into a computer. The final, processed results were used to create maps. The

boundary between sediment and bedrock is then marked using the 2D resistivity distribution map that was produced via data inversion. A dipole-dipole array was used for 2D electrical resistivity imaging across three traverses in order to examine lateral and vertical variations in subsurface conditions. The traverses used a 5 m dipole spacing, and deeper penetration was achieved by increasing the current and potential dipoles. The DIPRO software was used to process and reverse the acquired apparent resistivity measurements. After creating a preliminary model, this program reduced the difference between the model and the observed resistivity fields until a good fit was achieved. Taking into account the lateral and vertical continuity as well as the geometry of the image responses, 2D subsurface resistivity structures were studied in relation to subsurface lithology based on resistivity distribution, using known methods. Over a worn foundation, this showed a low continuous resistive subsurface layer with a resistivity of 120 Ωm , suggesting clay-rich material and a water-absorbing clayey layer. High horizontally and/or vertically continuous resistivity ($>1000 \Omega\text{m}$) was regarded as

fresh bedrock, whereas resistivity values ranging from 130 to 950 Ωm indicated a somewhat weathered and conductive fractured basement.

Results

The standard apparent resistivity data for traverses, the pseudo-section plots, and the corresponding profiles, traverses on the table, and maps accordingly transmitted the research results. This resistivity inversion model provides insights into the subsurface lithological characterisation of the region.

VES curve and Lithology Interpretation

The results of the VES geo-sounding curve were summarised and interpreted in Table 1 based on the lithology outlined, the thickness, depth, resistivity changes, rock layer and its numbers, and the VES numbers. The curves' forms, which correspond to the H, HA, and KH curve types, show three-layer subsurface patterns (figures 9-11). Subsurface lithologic sections were constructed along potential lines of VES locations based on the interpreted resistivity and thickness values of sounding curves.

Table 1: Summary of the study results and interpretation of the VES curve and lithology findings

VES No	No. of Layers	Ωm	Thickness (m)	Depth (m)	Lithology	Type Curve
1	4	188.9	1.1	1.1	Topsoil	KH
		283.8	4.5	5.6	Sandy Layer	
		96.5	6.9	12.5	Clayey Layer	
		298.8	-	-	Fresh Basement	
2	3	162.5	2.0	2.0	Topsoil	H
		3988.8	5.2	7.2	Laterite/Clay	
		9094.5	-	-	Fresh Basement	
3	4	191.8	1.0	1.0	Topsoil	HA
		123.0	1.2	2.2	Weathered Layer	
		124.0	5.3	7.5	Fractured Basement	
		325.4			Fresh Basement	

Pseudo sections Interpretation

The 2D pseudosection for this model in Figure 7 displays a lateral distance of 90 meters at 10-meter intervals. In order to improve resistivity distribution, this subsurface picture of lateral and vertical resistivity variation throughout the traverse set up in the research region was characterised using colour codes that ranged from green to blue to purple.

The resistivity value of the blue-colored zone is between 60 and 110 ohm-m, the light-green region is between 111 and 163 ohm-m, the yellowish-red region is between 165 and 214 ohm-m, and the redish-purple region is between 216 and 286 ohm-m. For traverse 1 examined, as shown in Figure 7, from 0.0 m to about 10 m vertical depth, 0m to 38m is light green colour seen as 70 ohm-m, then 40 m to 50 m

is redish purple colour seen as 170 ohm-m, then 61 m to 70 m bluish colour is about 89 ohm-m for lateral lengths. From 11 m - 20 m vertical depth, 20m -40m bluish colour is about 89 ohm-m, 41m -70m light green colour is about 150 – 270 ohm-m for lateral lengths. For 21m – 30m vertical depth, at 28 m – 65 m light green colour of about 150 ohm-m to 270 ohm-m for lateral lengths. From 31 m- 50m vertical depth, at 35m – 60m redish colour of about 490 ohm-m -874 ohm-m. Four geologic strata were identified by the 2D pseudo-section along the traverse: topsoil, worn layer, laterite clay, and fresh basement rock. Generally, It showed that the fracture zone which is one of the geologic structures for groundwater accumulation was chosen though with uncertainty as from the resistivity values, which varies from high (279-874 Ohm-m) to low (89-158 Ohm-m). The high resistivity values may be unconnected with suspected rock body as shown between stations 40 to 60 m with depth ranging from 1 meters to 5 meters. Also, a high resistivity values were observed between stations 30 and 65, with depth values ranging from 20 to 50 meters.

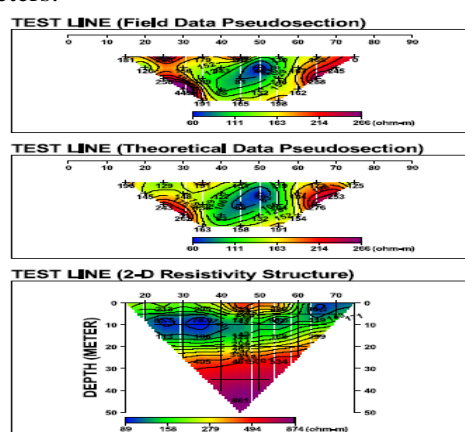


Figure 7: Traverse 1 model Pseudo-section outcome

Study area VES findings

VES 1, seen in Figure 8, has four strata: topsoil, a sandy layer, a clayey layer, and fresh basement rock. The resistivity varied from 189.9 to 283.8 ohm-m, while the thickness extended from 1.1 meters to infinity. The H curve type (Figure 8) described the three-layer geoelectric section, which was mostly composed of fresh basement rock, laterite/clay, and top loose soil from top to bottom with varying resistivity and thickness.

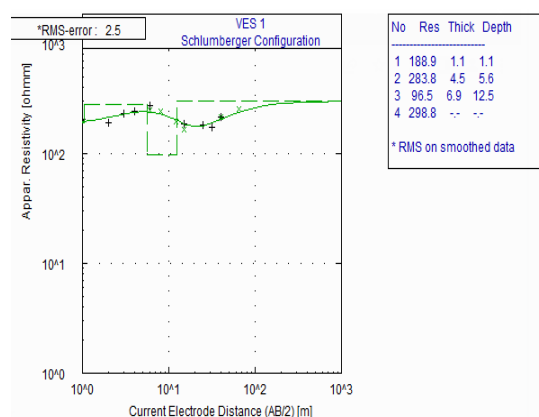


Figure 8: VES 1 curve type

VES 2 was shown in Figure 9 as having three layers, lithology of top soil, laterite clayey, and fresh foundation, resistivity ranging from 204.0 to 352 ohm-m, thickness ranging from 28 meters to infinity, and depth up to 28 meters until infinity.

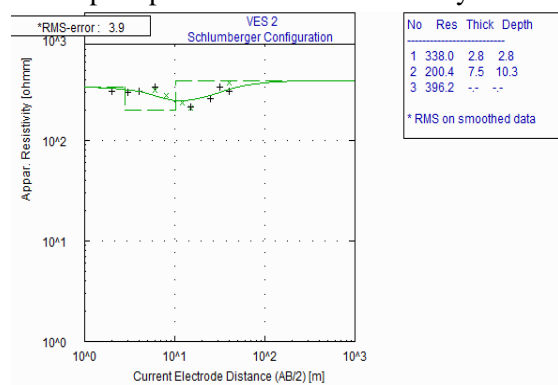


Figure 9: VES 2 curve type

The lithology of VES 3 was shown in Figure 10 to consist of four layers: top soil, weathered layer, fractured basement, and fresh basement. The resistivity ranged from 123.0 to 325.4 ohm-m, the thickness ranged from 1.0 meters to infinity, and the depth was up to 1.0 meters until infinity. Despite the low water zone classification of the area, VES 2 may be of interest and recommended for more groundwater exploration appreciable water with aquifer thickness and depth.

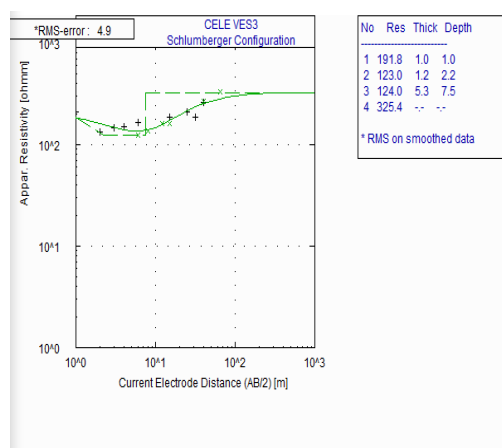


Figure 10: VES 3 curve type

High heterogeneity in the composition of the underlying geologic materials was shown by the appearance of several curve types at different locations within a region. The geology of the region may be roughly categorised as top soil, weathered layer, and fresh basement formations (figure.10) based on the interpreted resistivity values (table 1). Table 1 displays these formations' resistivity ranges. According to the findings of most sounding curves (table 1), the first layer's resistivity ranges from 189 to 338 ohm-m, and its thickness ranges from 1.0 to 2.8 meters. The northwest portion of the research region is characterised by strong resistivities and may be coated with migmatites. The second layer's thickness ranges from 1.2 to 4.5 m, and its resistivity mostly ranges from 123-284 ohm-m. Fresh basement rock was deduced to be the fourth subsurface layer of the geoelectric section. From top to bottom, the three-layer geoelectric section was composed of fresh basement rock, laterite/clay, and loose soil with varying resistivity and thicknesses, as shown by the H curve type. KH and HA curve types were used to characterise the 4-layer geoelectric section. High heterogeneity in the composition of the underlying geologic materials was shown by the appearance of several curve types at different locations within a region.

Discussion

Proper activities are put in place to enable Pore spaces and other structural deform play an important role in determination of quality and quantity to characterize a rock body that has capacity to store and transmit subsurface water for many uses. The primary objective of the research is aquifer delineation, using a selected approach to reduce costs, mitigate risks, and maximise available resources. For every civilisation to thrive healthily and productively,

access to fresh and drinkable groundwater is essential. The minimum amount of safe drinking water recommended for each person each day to maintain good health is thought to be around 100l, Falkenmark et al., (1989). Moreover, because of the local climate, geology, and topography, its relative abundance, distribution, and quality vary greatly over time and space. This research was conducted in 2022 and early 2023, identifying and establishing several hydro-geophysical characteristics, including aquifer resistivity, thickness, and depth, using curve types and pseudosection models. The sounding curve data indicated that the resistivity of the first layer ranges from 85.6 ohm-m to 162.5 ohm-m, with aquifer thicknesses between 1.4 m and 2.3 m, suggesting a favourable outcome if drilling is conducted. The resistivity of the second layer mostly ranges from 161.5 ohm-m to 6033.2 ohm-m, with a thickness between 2.5 m and 6.1 m. The second and third layers at depths of 3.9 - 8.4 m constitute the basement, exhibiting a very high resistivity (>150 ohm-m). The inversion results from the dipole-dipole electrical resistivity array reveal three electrical resistivity layers: (1) a superficial layer with relatively low resistivity (approximately 191.8 ohm-m), interpreted as topsoil; (2) a sandy layer (123.0 ohm-m – 3988.8 ohm-m); and (3) a weathered bedrock (96.5 ohm-m – 9094.5 ohm-m). (4) new basement. The integration of findings from the accepted model and curves highlighted the ambiguity in the region regarding water exploration, since the groundwater resources are classed as low to moderate prospective zones. Approximately 65% of the region is classified as having low groundwater potential, while only roughly 35% is deemed prospective for groundwater research, indicating a fairly poor groundwater prospect area. Onwuka and Adewsi (2023) illustrated that funding and cost issues hinder the attainment of specific technical objectives and additionally indicated that the 2D electrical resistivity of traverses interpreted as clay lithology was encountered in several intervals within the study area. Loke et al. (2010) observed that regions characterised by highly saturated clay often exhibit low resistivity values of less than 100 ohm-m. Similarly, Ganiyu et al. (2019) indicated that low resistive materials are interpreted as clayey substances. Coduto (1998) observed that rock materials under the groundwater table are typically saturated. Bowles (1984) asserted that the water table and its fluctuations are crucial considerations in structural studies. The evaluation and interpretation of VES (figures 7–10 and table 1) were incorporated into the study to verify structural deformation and identify weaknesses related to liquid transmissivity. The pseudo-sections derived from the dipole-dipole



and inferred lithology sections, interpreted from the VES data, are constructed by linking the soundings positioned along straight lines, revealing both weathered (2.1 - 6.1 m) and fresh basement layers. The clay intervals present, which are unsuitable for an effective aquifer due to their detrimental impact and impermeability, raise concerns. It is evident that VES 2, one of the three VES sites, should be re-examined prior to making additional recommendations for hand-dug well drilling, after a thorough analysis of the data to accurately characterise and assess the distribution of aquifer parameters in the research region.

Conclusions

The study highlighted the potential for groundwater exploration in Ayegbaju Ekiti, identifying promising zones through resistivity analysis and pseudosections. VES 2 demonstrates potential for further exploration due to its favorable aquifer characteristics, despite the area's low water zone classification.

Conflict of Interest

The authors hereby declare no conflict of interest.

Acknowledgments

The authors express gratitude to certain colleagues for offering analytical help, editing the work, and giving their publication as a model for this assessment. We really appreciate the constructive and invaluable feedback from the personnel of the Department of Geophysics and the anonymous reviewers for their assistance.

References

- Abu El-Magd, S. A., & El Dosouky, A. M. (2021). An improved approach for predicting the groundwater potentiality in the low desert lands; El-Marashda area, Northwest Qena City, Egypt. *Journal of African Earth Sciences*, 179, 104200. <https://doi.org/10.1016/j.jafrearsci.2021.104200>
- Alao, J. O., Yusuf, M. A., Nur, M. S. et al. (2023). Delineation of aquifer promising zones and protective capacity for regional groundwater development and sustainability. *SN Applied Sciences*, 5, 149. <https://doi.org/10.1007/s42452-023-05371-2>
- Alile, O. M., Ujuanbi, O., & Evbuomwan, I. A. (2011). Geoelectric investigation of groundwater in Obaretin-Iyanomon locality, Edo state, Nigeria. *Journal of Geology and Mining Research*, 3(1), 13–20.
- Amadi, A. N., Nwawulu, C. I., & Unuevho, N. O. (2011). Evaluation of the groundwater potential in Pompo Village, Gidan Kwano, Minna, using vertical electrical resistivity sounding. *British Journal of Applied Science & Technology*, 1(3), 53–66. <http://www.sciencedomain.org/abstract/53>
- Baloyi, L., Kanyerere, T., Muchingami, I., & Pienaar, H. (2024). Application of hydrogeophysical techniques in delineating aquifers to enhancing recharge potential areas in groundwater-dependent systems, Northern Cape, South Africa. *Water*, 16(18), 2652. <https://doi.org/10.3390/w16182652>
- Barker, R. D. (1980). Application of geophysics in groundwater investigations. *Water Survey*, 84, 489–492.
- Bayowa, O. G., Olorunfemi, M. O., Akinluyi, F. O., & Ademilua, O. L. (2014). Integration of hydrogeophysical and remote sensing data in the assessment of groundwater potential of the basement complex terrain of Ekiti State, southwestern Nigeria. *Ife Journal of Science*, 16(3).
- Bowles, J. E. (1984). *Physical and geotechnical properties of soils*. McGraw-Hill.
- Boyce, J. I., & Kaseoglu, B. B. (1996). Shallow seismic reflection profiling of waste disposal sites. *Geoscience Canada*, 23(1), 9–21.
- Coduto, D. P. (1998). *Geotechnical engineering: Principles and practices*. Prentice Hall.
- Dahlin, T. (1993). The automation of 2D resistivity surveying for engineering and environmental applications (Doctoral dissertation). *Department of Engineering Geology, Lund University, Sweden*.
- Dahlin, T., & Loke, M. H. (1998). Resolution of 2D Wenner resistivity imaging as assessed by numerical modeling. *Journal of Applied Geophysics*, 38, 237–249.
- Daramola, C. (2023). Exploration for groundwater using 2D imaging and vertical electrical sounding techniques (BSc Thesis). *Department of Geophysics, FUOYE*.
- Dobrin, M. B., & King, R. F. (1976). *Introduction to geophysical prospecting*. McGraw-Hill.
- Ehirim, C. N., & Ebeniro, J. O. (2010). Evaluation of aquifer characteristics and groundwater potentials in Awka, South East Nigeria using V-E sounding. *Asian Journal of Earth Sciences*, 3(2), 73–81.
- Eugene-Okorie, J. O., Obiora, D. N., Ibuot, J. C., & Ugbor, D. O. (2020). Geoelectrical investigation of groundwater potential and

- vulnerability of Oraifite, Anambra State, Nigeria. *Applied Water Science*, 10(10), 1–14.
- Fajana, A. O., Amosun, J., Abiodun, H., Tsado, J., & Owasanoye, A. (2024). Aeromagnetic and remote sensing application for groundwater exploration in Oye and its environs. *Journal of Innovation Science and Technology*, 2(1). Retrieved from <https://jist.fuoye.edu.ng/index.php/jist/article/view/25>
- Falkenmark, M., Lundqvist, J., & Widstrand, C. (1989). Macro-scale water requires micro-scale approaches. *Natural Resource Forum*, 13(4), 256–267.
- Ganiyu, S. A., Olurin, O. T., Oladunjoye, M. A., & Badmus, B. S. (2019). Investigation of soil moisture content over a cultivated farmland in Abeokuta Nigeria using electrical resistivity methods and soil analysis. *Journal of King Saud Science*, 32, 811–821. <https://doi.org/10.1016/j.jksus.2019.02.016>
- Hasan, M., Yanjun, S., Weijun, J., & Gulraiz, A. (2021). Estimation of hydraulic parameters in a hard rock aquifer using integrated surface geoelectrical method and pumping test data in southeast Guangdong China. *Geosciences Journal*, 25(2), 223–242. <https://doi.org/10.1007/s12303-020-0018-7>
- Hosny, M. M., Ezz El-Deen, A. A., Abdallah, A. A., Abdel Rahman, & Barseim, M. S. M. (2005). Geoelectrical study on the groundwater occurrence in the area southwest of Sidi Barrani, Northwestern Coast, Egypt. *Geophysical Society Journal*, 3(1), 109–118.
- Keller, G. V., & Frischknecht, F. C. (1966). *Electrical methods in geophysical prospecting*. Pergamon Press.
- Loke, M. H., Wilkinson, P. B., & Chambers, J. E. (2010). Parallel computation of optimized arrays for 2D electrical imaging surveys. *Geophysical Journal International*, 183(3), 1302–1315. <https://doi.org/10.1111/j.1365-246X.2010.04796.x>
- Mousa, D. A. (2003). The role of 1-D sounding and 2-D resistivity inversions in delineating the near-surface lithologic variations in Tushka area, south of Egypt. *Geophysical Society Journal*, 57–64.
- Nigm, A. A., Elterb, R. A., Nasr, F. E., & Thobaity, H. M. (2008). Contribution of ground magnetic and resistivity methods in groundwater assessment in Wadi Bany Omair, Holy Makkah Area, Saudi Arabia. *Egyptian Geophysical Society Journal*, 6(1), 67–79.
- Obiora, D. N., Alhasan, U. D., Ibut, J. C., & Okeke, F. N. (2016). Geoelectric evaluation of aquifer potential and vulnerability of northern Paiko, Niger State, Nigeria. *Water Environment Research*, 88(7), 644–651.
- Olorunfemi, M. O., Idonigie, A. I., Coker, A. T., & Babadiya, G. E. (2004). The application of the electrical resistivity method in foundation failure investigation: A case study of O.A.U Dental Clinic. *Global Journal of Geophysical Science*, 2(1), 139–151. <https://doi.org/10.4314/gjgs.v2i1.18689>
- Oyedele, K. F., Ayolabi, E. A., Adeoti, L., & Adegbola, R. B. (2009). Geophysical and hydrogeological evaluation of rising groundwater level in the coastal areas of Lagos, Nigeria. *Bulletin of Engineering Geology and the Environment*, 68, 137–143.
- Walraevens, K., et al. (2025). Assessing the Potential of Volcanic and Sedimentary Rock Aquifers in Africa. *Water*, 17(1), 109. <https://doi.org/10.3390/w17010109>
- Zenande, N., Adesola, G.O., & Madi, K. (2024). *Sustain. Water Resour. Manag*, 10, 188. <https://doi.org/10.1007/s40899-024-01166-4>